VEGFR2 Trafficking by KIF13B Is a Novel Therapeutic Target for Wet Age-Related Macular Degeneration

Stephen B. Waters,[1] Christopher Zhou,[1] Tara Nguyen,[2] Ruth Zelkha,[2] Hyun Lee,[3] Andrius Kazlauskas,[2,4] Mark I. Rosenblatt,[2] Asrar B. Malik,[1] and Kaori H. Yamada[1,2]

[1]Department of Pharmacology and Regenerative Medicine, University of Illinois College of Medicine, Chicago, Illinois, United States
[2]Department of Ophthalmology and Visual Sciences, University of Illinois College of Medicine, Chicago, Illinois, United States
[3]Biophysics Core & Department of Pharmaceutical Sciences, University of Illinois College of Medicine, Chicago, Illinois, United States
[4]Department of Physiology and Biophysics, University of Illinois College of Medicine, Chicago, Illinois, United States

Correspondence: Kaori H. Yamada, Department of Pharmacology and Regenerative Medicine, University of Illinois College of Medicine, Chicago, IL, 60612, USA; horiguch@uic.edu.

Received: July 26, 2020
Accepted: January 13, 2021
Published: February 3, 2021

Citation: Waters SB, Zhou C, Nguyen T, et al. VEGFR2 trafficking by KIF13B is a novel therapeutic target for wet age-related macular degeneration. *Invest Ophthalmol Vis Sci.* 2021;62(2):5. https://doi.org/10.1167/iovs.62.2.5

Purpose. Vascular endothelial growth factor (VEGF) and its receptor VEGFR2 are promising therapeutic targets for wet age-related macular degeneration (AMD). As a topically applicable option, we developed the peptide KAI to selectively interfere with VEGFR2 trafficking to the cell surface where it receives VEGF. This study sought to determine the efficacy of KAI in the mouse model of choroidal neovascularization (CNV).

Methods. The specificity of KAI was tested by surface plasmon resonance. The drug delivery was analyzed by cryosection and the ELISA after treatment of KAI eyedrop to the mouse eyes. For the laser-induced CNV model, mice with laser-induced ruptures in Bruch's membrane received daily treatment of KAI eyedrop or control peptide. The other groups of mice received intravitreal injection of anti-VEGF or IgG control. After two weeks, CNV was quantified and compared.

Results. First, we showed the specificity and high affinity of KAI to VEGFR2. Next, biodistribution revealed successful delivery of KAI eyedrop to the back of the mouse eyes. KAI significantly reduced the disease progression in laser-induced CNV. The comparison with current therapy suggests that KAI eyedrop is as effective as current therapy to prevent CNV in wet AMD. Moreover, the genetic deletion of a kinesin KIF13B, which mediates VEGFR2 trafficking to the cell surface, confirmed the pivotal role of KIF13B in disease progression of wet AMD and neovascularization from choroidal vessels.

Conclusions. Taken together, pharmacologic inhibition and genetic deletion complementarily suggest the therapeutic possibility of targeting VEGFR2 trafficking to inhibit pathological angiogenesis in wet AMD.

Keywords: wet AMD, angiogenesis, eyedrop, therapy, VEGFR2

Angiogenesis, the growth of new blood vessels from preexisting vasculature, is implicated in the pathogenesis of a variety of diseases, such as cancer and eye diseases.[1,2] A therapeutic strategy targeting angiogenesis started in cancer therapy.[3] Because vascular endothelial growth factor A (VEGF A) is elevated in cancer and eye diseases, removing VEGF using its antibody was a striking strategy for cancer.[4] However, anti-VEGF therapies have proven to be of limited benefit for cancer patients due to the development of resistance to the therapies.[5,6] Cancer and eye diseases such as wet age-related macular degeneration (AMD) have an important common trait, elevated expression of VEGF induces abnormal leaky angiogenesis.[1] In fact, anti-VEGF therapies for eye diseases actually improve vision in the majority of patients with wet AMD.[3,7] However, there are still patients who do not respond to anti-VEGF therapies.[8,9] Multiple attempts have been made to tackle nonresponsiveness such as switching the anti-VEGF drugs with other drugs.[8,10] Thus novel strategies targeting VEGF/VEGFR2 pathway with different mechanisms constitute a fertile opportunity for drug development. Our strategy is based on our recent findings[11,12] and other research groups[13–18] that VEGFR2 trafficking is necessary for angiogenesis. In contrast to current anti-VEGF therapies, our strategy is to inhibit angiogenesis by limiting the amount of VEGFR2 at the cell surface of the endothelial cells (ECs) in growing vessels, where VEGFR2 receives the VEGF ligand.

VEGFR2 signaling is tightly regulated by its availability at the endothelial cell surface.[17,19] On binding of VEGF, VEGFR2 is phosphorylated and internalized.[18,19] The fate of internalized VEGFR2 depends on the molecules with which it associates.[17] VEGFR2 is either shuttled to lysosomes for degradation,[20–22] or recycled back to adherens junctions (AJs) to interact with VE-cadherin to close AJs and restore the quiescent phenotype.[13,23] VEGFR2 is also observed at the leading edge of migrating EC,[24] and

Copyright 2021 The Authors

This work is licensed under a Creative Commons Attribution-NonCommercial-NoDerivatives 4.0 International License.

Investigative Ophthalmology & Visual Science

localization of VEGFR2 at filopodia of tip cells is essential to sense VEGF gradient and to induce directional EC migration toward VEGF.[14,25,26] Therefore the dynamic trafficking of VEGFR2 is likely important for angiogenesis.[11–13,16,18] However, mechanisms mediating trafficking of VEGFR2 to filopodia of migrating/sprouting EC are largely unknown. As a possible mechanism mediating the translocation of VEGFR2, we have investigated the role of KIF13B, a kinesin motor on microtubules.[27] We showed VEGFR2 interacts with KIF13B, which transports VEGFR2 to cell surface.[12] The trafficking of VEGFR2 by KIF13B is critical for VEGF-induced angiogenesis.[12] The inhibition of VEGFR2 trafficking by disruption of the interaction between KIF13B and VEGFR2 showed an inhibitory effect on tumor angiogenesis and tumor growth.[11] We posit from this concept that inhibition of KIF13B-mediated VEGFR2 trafficking will be an effective therapy in mitigating pathological angiogenesis seen in cancer and blinding eye diseases, such as wet AMD. In this article, we show the efficacy of our strategy to inhibit pathological angiogenesis in wet AMD animal model, laser-induced CNV.

Methods

Peptides

Biotin-KAI and biotin-ctrl were synthesized by a custom synthesized service (Thermo Fisher Scientific, Waltham, MA, USA).

Antibodies

Antibodies used for this study include rabbit antibodies against VEGFR2 (Cell Signaling Technology, Danvers, MA, USA) and GAD65 (Abcam, Cambridge, MA, USA), goat antibody against Centaurin A (Santa Cruz Biotechnology, Dallas, TX, USA), mouse antibodies against rhodopsin (Millipore, Burlington, MA, USA) and glutamine synthetase (BD Bioscience, Franklin Lakes, NJ, USA). To neutralize VEGF in the mouse laser-induced CNV model, a mouse-specific antibody against VEGF (512807; BioLegend, San Diego, CA, USA) and the IgG control (400515; BioLegend) was purchased from the same company. Aflibercept was obtained from the eye clinic adjacent to the Department of Ophthalmology at UIC. Other reagents used were isolectin B4 (Vector Laboratories, Burlingame, CA, USA), Alexa 594 anti-rabbit antibody, Alexa 488 anti-mouse antibody, Alexa 488-streptavidin (Invitrogen, Carlsbad, CA, USA), and HRP-conjugated secondary antibodies (Jackson Immunoresearch Laboratories, West Grove, PA, USA).

Animals

C57BL mice were purchased from the Jackson Laboratory. To obtain KIF13B knockout mice, KIF13B-floxed mice (*KIF13B*^{tm1a} in Supplementary Fig. S3A) from the European Mouse Mutant Archive was crossed with flippase1 (flp1)-expressing mice (The Jackson Laboratory), followed by crossing with CMV-Cre mice (The Jackson Laboratory). *KIF13B*$^{tm1d/tm1d\ (KO/KO)}$/CMV-Cre(+) mice were confirmed by PCR (Supplementary Fig. S3B). The primers used are: KIF13B-F (5′-TCC CAA AAC ATG GTC AGG TG-3′), KIF13B-R (5′- GAC AGT GGG GGT CAG TGA TG-3′), CAS-R (5′- TCG TGG TAT CGT TAT GCG CC-3′), Cre-F (5′- GCG GTC TGG CAG TAA AAA CTA TC-3′), and Cre-R (5′- GTG AAA CAG CAT TGC TGT CAC TT-3′). All animal experiments were carried out in compliance with the relevant laws, and institutional guidelines and were approved by animal ethics committees.

Pull-Down Assay

The human umbilical vein endothelial cells (HUVEC) were obtained from Lonza, cultured in EGM2 (Lonza Group, Basel, Switzerland), used between passage 3 to 6. Biotin-KAI and biotin-ctrl were immobilized on the streptavidin beads. The lysate of HUVEC was incubated with biotin-KAI or biotin-ctrl on the beads. After washing, the proteins bound on the beads were analyzed by Western blotting with antibodies against VEGFR2 or Centaurin A.

Mass Spectrometry

Biotin-KAI and biotin-ctrl were immobilized on the streptavidin beads. The membrane fraction was isolated from the mouse lung using Mem-PER Plus Membrane Protein Extraction Kit (Pierce; Thermo Fisher Scientific), according to the manufacture's protocol. The lysate of the membrane fraction was incubated with biotin-KAI and biotin-ctrl on the beads to isolate binding proteins. The binding proteins were separated by SDS-PAGE, visualized by Coomassie Blue staining. The bands specific to biotin-KAI compared to biotin-ctrl were digested and sent to Taplin Mass Spectrometry Facility at Harvard Medical School. After the digestion of the proteins by the proteinases, the peptide fragments were analyzed based on the molecular weight and charge to determine the parental proteins. The proteins bound to biotin-ctrl were also analyzed as references. The unique proteins in the pull-down with biotin-KAI that were not found in biotin-ctrl were selected. The number of the total and unique peptide fragments, the name of the determining gene, cross-correlation (XCorr), and delta correlation (ΔCorr) were shown in the table. Cross-correlation is a score of the number of fragment ions that are common to two different peptides with the same precursor mass and calculates the cross-correlation score for all candidate peptides queried from the database. The higher score is better. Delta correlation is a measure of the specificity of the fit. The smaller number implies a better fit.

Surface Plasmon Resonance (SPR)

Two peptides, biotin-KAI and biotin-ctrl (Pierce custom peptide synthesis; Thermo Fisher Scientific), were diluted to 50 µg/mL in commercial buffer HBS-EP (10 mM Hepes, pH 7.4, 150 mM NaCl, 3 mM EDTA, and 0.05% surfactant P-20) from GE Healthcare. Biotin-KA1 and biotin-ctrl were immobilized on streptavidin-coated sensor chip SA on flow channels 2 and 4, respectively using a Biacore T200 instrument (GE-Healthcare, Chicago, IL, USA). Blank surfaces without any immobilization were used as references on flow channels 1 and 3. Recombinant proteins of the cytosolic domains of receptor tyrosine kinases (RTKs) (VEGFR2, PDGFRA, PDGFRB, and EGFR), expressed in Sf9 insect cells and isolated as active kinases, were purchased from Fisher Scientific. These testing proteins were diluted to a series of increasing concentrations ranging from 5.1 nM to 200 nM at 2.5-fold dilution in HBS-EP buffer and applied to all four channels at a 25 µL/min flow rate at 25°C. The single-cycle kinetic method was run, and real-time response units were monitored. Sensorgrams were double referenced with the blank channel and zero concentration responses and fitted with 1 to 1 Langmuir kinetic equation embedded in the Biacore T200 evaluation software v3.0.

Laser-Induced Choroidal Neovascularization

Under anesthesia, the pupils of C57BL/6 mice were dilated, and the eye lubricant was applied to the eyes. Because the even focus was essential for producing consistent laser burns and CNV lesions, the optic nerve was positioned in the center of the view field, and the alignment of the axis of both the mouse eye and the lens was confirmed by evenly bright and clear observation of the reflection of the retinal nerve fibers in all direction.[28] Using Phoenix Micron IV and Phoenix Image-Guided Laser System with 532 nm laser (Phoenix Technology Group, Pleasanton, CA, USA), laser burns of 200 to 355 mW output, 50 µm fixed diameter, 70 msec duration were applied on the eyes.[28,29] All groups of mice in Figures 1D to 1F received laser 355 mW output. To reduce the incidence of fused lesions, we reduced the laser power, and all groups of mice in Figures 3 and 4A to 4D received laser 200 mW output. Four laser burns were applied on the right eyes using a laser focused on the retinal pigment epithelium (RPE). The presence of a bubble confirms the success of the laser impact.[28,29] For the peptide-treated groups (groups 1, 2, and 3 from left in Figs. 3B and 3C), eye drops of KAI (5 µg/eye in 5 µL PBS) or ctrl (5 µg/eye) were applied daily on the eyes with laser burns. Group 4 was treated with eye drops of KAI (5 µg/eye in 5 µL PBS) daily from day 7 to day 14. For the groups treated with anti-VEGF antibody and IgG (groups 5 and 6), the intravitreal injection was performed during anesthesia just after laser induction. Group 7 received the intravitreal injection of anti-VEGF antibody on day 7. Eyes were locally anesthetized with proparacaine, and an initial hole was made under the limbus with a 33-gauge needle. Thereafter, an anti-VEGF antibody or IgG (2 µg in 2 µL PBS) was intravitreally injected through the initial hole using a sharpened-glass capillary under the dissection microscope. At 7 days and 14 days after laser burns, the eyes were analyzed with optical coherence tomography (OCT) imaging and fluorescence angiography. At 14 days after laser burns, the eyes were isolated, and the choroidal flat mount was stained with DyLight 594-ILB4 (Thermo Fisher Scientific) to visualize the CNV lesion. The area of CNV lesions was measured in Image J. Cross-sectional OCT scans of the lesion showing the choroidal fibrovascular tissue formation (marked by an orange dot line in Fig. 1D) was measured, and the average area per mouse was plotted in the graph. The surface area of CNV in the choroidal flat mount was also measured using staining of ILB4, and the average per mouse was plotted in the graph. The lesion with a hemorrhage bigger than the size of the original laser burn was excluded for both analyses of OCT and ILB4. If OCT analysis was unable because of mild temporary cataract by anesthesia, the mouse was excluded at the time point. If the isolated choroidal tissue was damaged during the isolation step, the mouse was excluded from the analysis of ILB4. The fused lesions and outlier lesions were included in the analysis. In the case of fused lesions, the area of entire lesions was measured together, divided by the number of lesions, and averaged with other lesions per mouse.

Biodistribution

The right eyes of C57BL/6 mice were treated with biotin-KAI (5 µg/eye in 5 µL PBS). At different time points (10 minutes, 30 minutes, 1 hour, and 2 hours), mice were sacrificed, and the eyes were isolated to freeze in optimal cutting temperature compound. The cryosection of the eyes was stained with DyLight 594-ILB4 and Alexa 488-streptavidin. The confocal images were all taken in the same microscope settings such as gain and scanning time.

To measure the amount of peptide in the eyes, the right eyes of C57BL/6 mice were treated with biotin-KAI (5 µg/eye in 5 µL PBS) or just PBS 5 µL (no-peptide control). At 30 minutes after treatment, mice were sacrificed, and fresh eyes were dissected into cornea, retina, and choroid. The amount of biotin-tagged peptides from these fluids and tissues were analyzed by the biotin ELISA assay. Briefly, the ELISA plate was coated with biotinylated protein (0.02 µg/well). Nonspecific binding was blocked by 0.2% I-Block and incubated with streptavidin-HRP and standard biotin (known concentration of biotin-KAI), or streptavidin-HRP and tissue lysate. After washing with PBS 0.025% Tween 20, the reaction was developed with TMB and stopped with 2M sulfuric acid. Absorbance at 450 nM was read with a microplate reader. The amount of biotin-KAI µg/mg tissue was measured in both peptide-treated samples and no-peptide controls. The average amount of biotin in no-peptide controls was subtracted from the amount of biotin-KAI in the tissues. Average biotin-KAI µg/mg tissue ± SE was described in the text ($N = 6$).

Choroidal Sprouting

The eyes from C57BL/6, *KIF13B*^{WT}, and *KIF13B*^{KO} mice were used for choroidal sprouting assay as described.[30] The eyes were isolated and dissected under the dissection microscope. The cornea, lens, and retina were removed. Because the choroidal fragments from the central region adjacent to the optic nerve head sprout more slowly and less consistently than those from the peripheral region adjacent to the ora serrata,[30] we discarded the central area around the optic nerve (1 mm in diameter). The peripheral choroid-scleral complex was dissected into approximately 0.3 to 0.6 mm^2 and embedded in the Matrigel. The choroid fragments were cultured with EC culture medium (EGM2 supplemented with 5% FBS and pen-strep) for two days, serum-starved with EBM2 supplemented with 0.1% BSA for four hours, and cultured with EBM2 supplemented with 2% FBS, GA-1000, hydrocortisone, and ascorbic acid, without any growth factors until day 7. Consistent with the literature,[30] intra-animal variation and interanimal variation was small if we dissected the same radial distance from the optic nerve head with minimum damage to the tissue fragments. We dissected about four or five pieces of fragments from each mouse, repeated the experiments three times, and plotted the individual area of sprouting from each mouse in the graph. To test the effect of Aflibercept, 12 choroidal fragments were dissected from the same animal, embedded in Matrigel, and cultured as described above for two days. After serum starvation on day 2, Aflibercept (40 mg/mL, 348 µM) was diluted and added to the culture at 30 nM and 100 nM from day 2 to day 7. The experiment was repeated three times. The area of sprouting was measured and the individual area of sprouting from each tissue fragment from three independent experiments was plotted in the graph as mean ± SE.

Results

KAI Is Specific to VEGFR2

We have previously reported that the small peptide named as Kinesin-derived angiogenesis inhibitor (KAI), inhibits the interaction between KIF13B and VEGFR2, thus inhibits

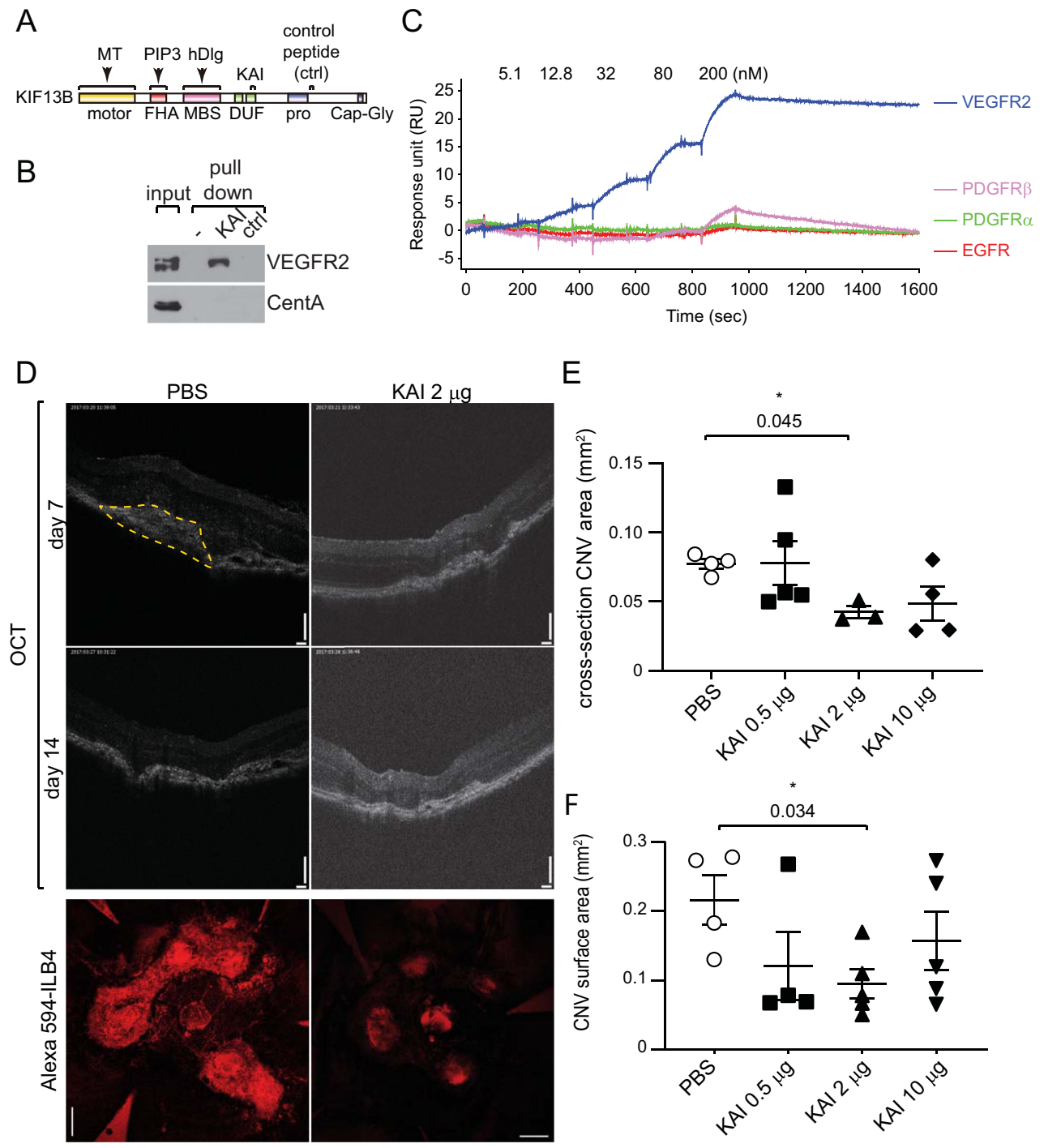

Figure 1. KAI, a specific inhibitor of KIF13B-mediated VEGFR2 trafficking, inhibits neovascularization in wet AMD. (**A**) Schematic showing the domains of KIF13B, binding sites of other cargoes, and peptides derived from KIF13B. (**B**) Pull-down assay showing the interaction of VEGFR2 with KAI but not with ctrl. Biotin-KAI and ctrl were immobilized on the streptavidin beads and incubated with the lysate of HUVEC. The proteins bound on the beads and input in the cell lysate were detected with the antibodies against VEGFR2 and CentA. VEGFR2 interacted with KAI but not with ctrl. Both peptides did not interact with CentA. (**C**) Binding affinity (K_D) of KAI to RTKs analyzed by SPR. Biotin-tagged KAI and ctrl were immobilized on the streptavidin-chip and tested for affinity with recombinantly expressed cytosolic kinase domains of VEGFR2, PDGFRα, PDGFRβ, and EGFR (Fisher Scientific). VEGFR2 showed a high affinity to KAI ($K_D = 6.8 \pm 0.6$ nM), whereas other RTKs had negligible ($K_D > 200$ nM) or no binding. All RTKs did not interact with ctrl. (**D, E, F**) The dose-dependent effect of KAI was tested by intravitreal injection of KAI 0.5 μg, 2 μg, and 10 μg after laser photocoagulation. Represent images of OCT and staining of the flat-mount of choroid/sclera with DyLight594-ILB4 were shown. *Bars:* 100 μm in OCT, 200 μm in ILB4 staining. $N = 5$ mice were used for PBS, KAI 0.5 μg, 2 μg, and 10 μg groups. Four laser burns were induced in each mouse, and the average neovascularization area per mouse was shown in graphs **E** and **F**. The cross-section of the CNV area in OCT (*orange dashed line*) was measured and plotted in graph E. *$P = 0.045$ one-way ANOVA, compared to PBS. ($N = 4, 5, 3, 4$ mice for PBS, 0.5 μg, 2 μg, 10 μg KAI, respectively. Mice with mild cataract due to anesthesia were unable to be monitored by OCT and were omitted from the measurement.) CNV surface area of the flat-mount was assessed by the area of ILB4-staining and plotted in graph **F**. *$P = 0.034$, one-way ANOVA. ($N = 4, 4, 5, 5$ mice in PBS, 0.5 μg, 2 μg, 10 μg KAI, respectively. Two choroidal tissues were damaged during the preparation of flat mount, and we were unable to assess the area of CNV.)

Investigative Ophthalmology & Visual Science

VEGF-induced angiogenesis in vitro and cancer model.[11] KAI is aa 1238-1260 of human KIF13B (Fig. 1A), designed from the minimum binding site to VEGFR2.[11] A peptide from aa 1650-1672 of human KIF13B (named as ctrl) is used as a negative control, because ctrl does not overlap with the binding sites for any cargoes of KIF13B. Both of the peptides are water-soluble, cell-permeable, 23 aa peptides, and synthesized with biotinylated N-terminus and amidated C-terminus (Thermo Fisher Scientific).

To apply these peptides for a disease model of an animal, we further tested the specificity of the peptides. First, we tested whether KAI is specific to VEGFR2 and does not bind to other cargo of KIF13B by pull-down assay (Fig. 1B). Biotinylated peptides were immobilized on the streptavidin beads and incubated with lysate of HUVEC to pull down VEGFR2. As we have shown before, KAI interacts with VEGFR2, whereas ctrl did not (Fig. 1B). One of the other cargoes for KIF13B, Centaurin alpha (CentA), an adaptor connecting PIP3 and KIF13B,[31] was also tested for the binding with these peptides (Fig. 1B). CentA was known to bind to the FHA domain of KIF13B (Fig. 1A)[31]; the binding site was distinct from KAI or ctrl sequence. Although CentA was detected in cell lysate, it did not show any interaction with these peptides (Fig. 1B).

To further test the specificity of KAI, we used pull-down of proteins from lung lysate using KAI or ctrl immobilized on streptavidin beads followed by mass spec analysis of the binding proteins, and detected KIF13B, VEGFR2, and NRP1 (number of hits was 28, 11, and 5, respectively), as a binding complex (Supplementary Fig. S1A). The important receptors for angiogenesis, Tie2, Par1, S1PR1, and FGFR were not found, consistent with the specificity as shown in.[11] Other cargoes for KIF13B (CentA and hDlg) were also not found, consistent with Fig. 1B. Some RTKs (PDGFRα, PDGFRβ, and EGFR) were identified because of the similarity of the kinase domain (number of hits was 6, 5, and 1, respectively) (Supplementary Fig. S1A), whereas these kinases did not interact with ctrl. Then we tested the direct binding of KAI with each RTK by SPR using Biacore T200 (Fig. 1C and Supplementary Figs. S1B, S1C). First, biotinylated peptides KAI and ctrl were immobilized on the streptavidin-coated sensor chip surface. Recombinant protein of the cytosolic domain (789-1356 aa) of VEGFR2 was tested for the affinity to each immobilized peptide (Supplementary Figs. S1B, S1C). VEGFR2 showed a very tight binding affinity to KAI, whereas even a high concentration of VEGFR2 did not show any binding to the ctrl peptide. Then the affinity of the recombinant proteins of RTKs to KAI was also measured for direct comparison (Fig. 1C). VEGFR2 bound very tightly to KAI at K_D value of 6.8 nM (Fig. 1C). SPR study also revealed very weak binding of PDGFRβ to KAI at negligible K_D, whereas PDGFRα and EGFR did not bind to KAI (Fig. 1C). These data indicate a high degree of specificity of KAI to VEGFR2.

Kai Inhibits Neovascularization in the CNV Model of Wet AMD

First, to test the concept of the inhibition of angiogenesis, we tested intravitreally injected KAI in laser-induced CNV. Wet AMD is characterized by the growth of the blood vessels from the choroid, which penetrate through Bruch's membrane into the subretinal area. Laser-induced CNV is a well-established experimental model for wet AMD, the disruption of Bruch's membrane by a laser beam promotes the growth of new choroidal vessels into the retina thus mimicking the pathological conditions of wet AMD.[28,29] C57BL/6 WT mice (seven weeks old) received laser burn, followed by intravitreal injection of KAI (0.5 µg, 2 µg, or 10 µg in 2 µL PBS) or PBS vehicle (2 µL) (Figs. 1D–1F). Optical coherence tomography (OCT) (Fig. 1E), and staining with ILB4 were used to assess neovascularization (Fig. 1F). Comparing to the PBS control, intravitreally injected KAI (2 µg) significantly inhibited CNV. The effect of 0.5 µg and 10 µg of KAI was not significant.

Delivery of Topically Applied KAI to the Back of the Mouse Eyes

Next, the question arises whether the peptides can be delivered into the damaged area by eye drops. To analyze the biodistribution of KAI in mouse eyes, we treated the eyes of C57BL/6 with biotin-KAI eye drop (5 µg/eye). At the different time points after treatment of biotin-KAI eye drop (10 minutes, 30 minutes, 1 hour, and 2 hours), the biodistribution of biotin-KAI was analyzed by staining of cryosection with Alexa 488-streptavidin and counterstaining with DyLight594-ILB4 (Fig. 2A). KAI was detected in the retina and choroid at 30 minutes and cleared from tissue at one to two hours after administration. Higher magnification of the retina after 30 minutes of administration of biotin-KAI further revealed the colocalization of biotin-KAI with ILB4, the endothelial marker at the choroidal vessel (arrowhead). Biotin-KAI was also observed in the area between RPE and a pigmented layer (choroid) (arrows). Expression of VEGFR2 in the same area was detected in the healthy eyes (Supplementary Fig. S3C), which is consistent with the literature showing the preferential expression of VEGFR2 in the choriocapillaris right adjacent to the RPE layer.[32] This result suggests the successful delivery of the peptides by eye drops to the disease area of the wet AMD.

To quantify the amount of KAI in each part of mouse eyes, we treated the eyes of C57BL/6 with biotin-KAI eye drop (5 µg/eye). At 30 minutes after treatment of biotin-KAI eye drop, the eyes were isolated and dissected into cornea, retina, and choroid/sclera. The amount of biotin-KAI was measured by competitive biotin ELISA assay,[33] using the standard curve of known concentration of biotin-KAI. At 30 minutes after treatment with an eye drop, 0.23 ± 0.11, 0.67 ± 0.30, and 0.92 ± 0.43 µg/mg tissue of biotin-KAI were detected in cornea, retina, and choroid, respectively.

Efficacy of KAI Eye Drop in Laser-Induced CNV

Then, we tested the efficacy of KAI as an eye drop in the mouse wet AMD model. Control peptide, which does not inhibit angiogenesis,[11] was used as a negative control. C57BL/6 (7 weeks old) mice received laser burns of similar size in all conditions (Fig. 3A, top panel, day 1). After laser-burn, mice were treated with daily treatment (day 1 to day 14) of either ctrl or KAI eye drop (2~5 µg/eye). Fluorescein angiography and OCT were used to monitor the lesions and leakage at day 7 and day 14. On day 14, the staining of flat mount choroid with ILB4 was used to assess neovascularization. Compared to the ctrl, KAI eye drop significantly reduced the area of choroidal neovascularization measured by OCT (cross-section) and ILB4 (surface area of CNV) (Figs. 3A–3C).

Investigative Ophthalmology & Visual Science

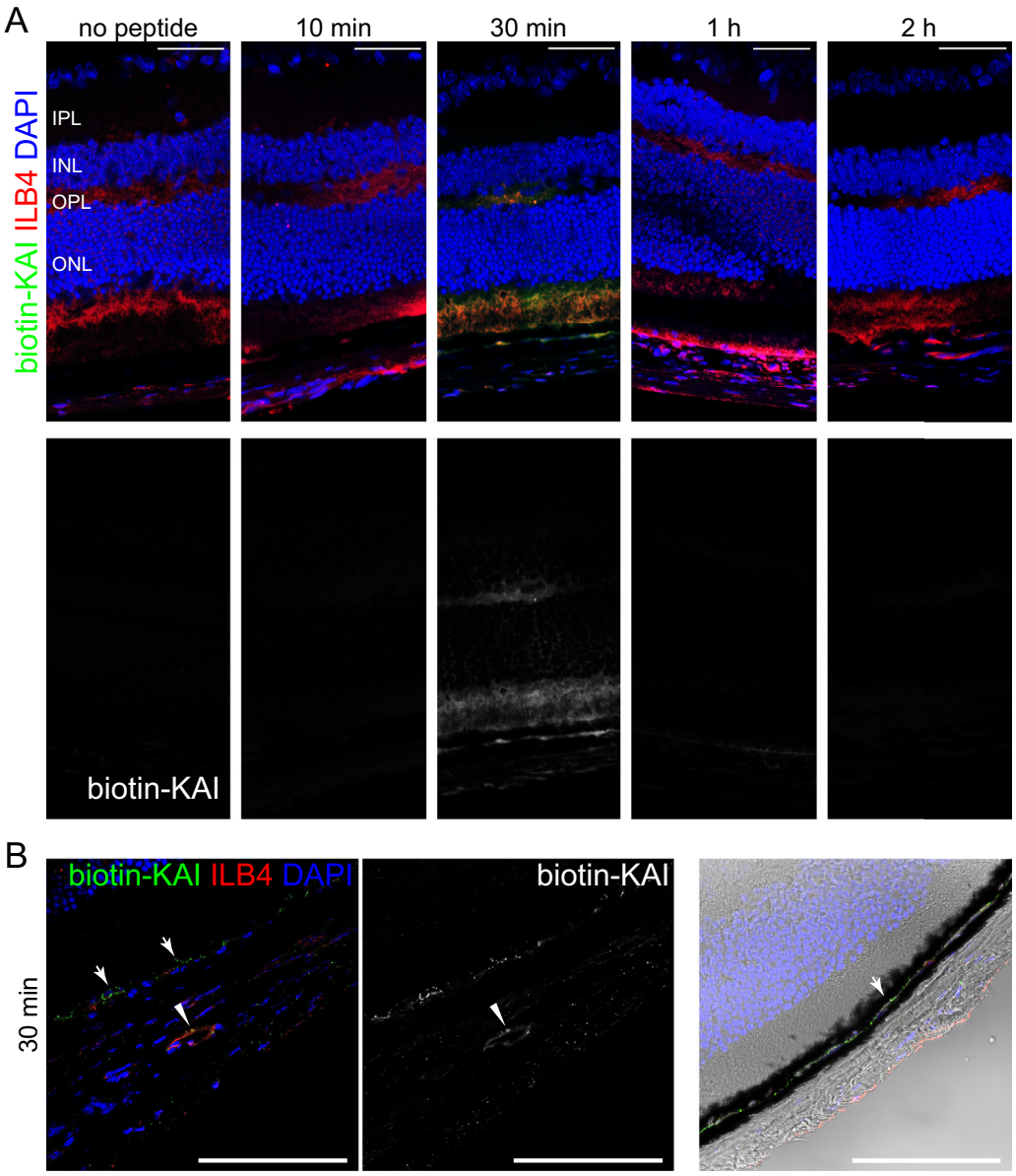

Figure 2. Topically applied KAI eye drop is successfully delivered to the back of the eyes. (**A, B**) Biodistribution of KAI in mouse eyes. After treatment of biotin-KAI eye drop (5 µg/eye) in the eyes of C57BL/6 (10 minutes, 30 minutes, 1 hour, and 2 hours), the biodistribution of biotin-KAI was analyzed by staining of cryosection with Alexa 488-streptavidin and counterstaining with DyLight594-ILB4. *Scale bar:* 50 µm. The magnified figure of the choroid was shown in **B**. Biotin-KAI was detected in the pigmented layer (*arrow*) and in the choroidal vessels (*arrowhead*), which were also stained with endothelial marker ILB4. *Scale bar:* 100 µm.

The current therapy of wet AMD is the intravitreal injection of anti-VEGF antibodies or anti-VEGF recombinant protein.[34,35] We tested the efficacy of the eye drop of KAI and intravitreal injection of mouse-specific anti-VEGF antibody (Figs. 3B and 3C and Supplementary Fig. S2). After laser burn, KAI groups and the ctrl group received daily treatment of eye drop (Fig. 3A), whereas the anti-VEGF group and IgG group received one-time intravitreal injection of antibodies (2 µg/eye) on day 1 (Supplementary Fig. S2). Compared to IgG control, the anti-VEGF antibody inhibited CNV, however, there is relatively higher variation in mice that received an intravitreal injection (Figs. 3B, 3C). Treatment of KAI eye drop showed more reliable inhibition of neovascularization for many mice. We further examined the effect of KAI for the regression of developed CNV and compared the effect of regression with an anti-VEGF antibody (Figs. 3B and 3C and Supplementary Fig. S2). KAI day 7 group received daily treatment of KAI (5 µg/eye) from day 7 to day 14. The anti-VEGF day 7 group received an intravitreal injection (2 µg/eye) on day 7. Interestingly, the treatment of KAI eye drop from day 7 to day 14 was also as effective to regress neovascularization (Figs. 3B and 3C). The intravitreal injection of the anti-VEGF antibody on day 7 was also effective (Fig. 3B). Taken together, KAI showed significant inhibition (prevention and regression) of CNV in this model of wet AMD, with comparable efficacy with current therapy, anti-VEGF antibody.

Investigative Ophthalmology & Visual Science

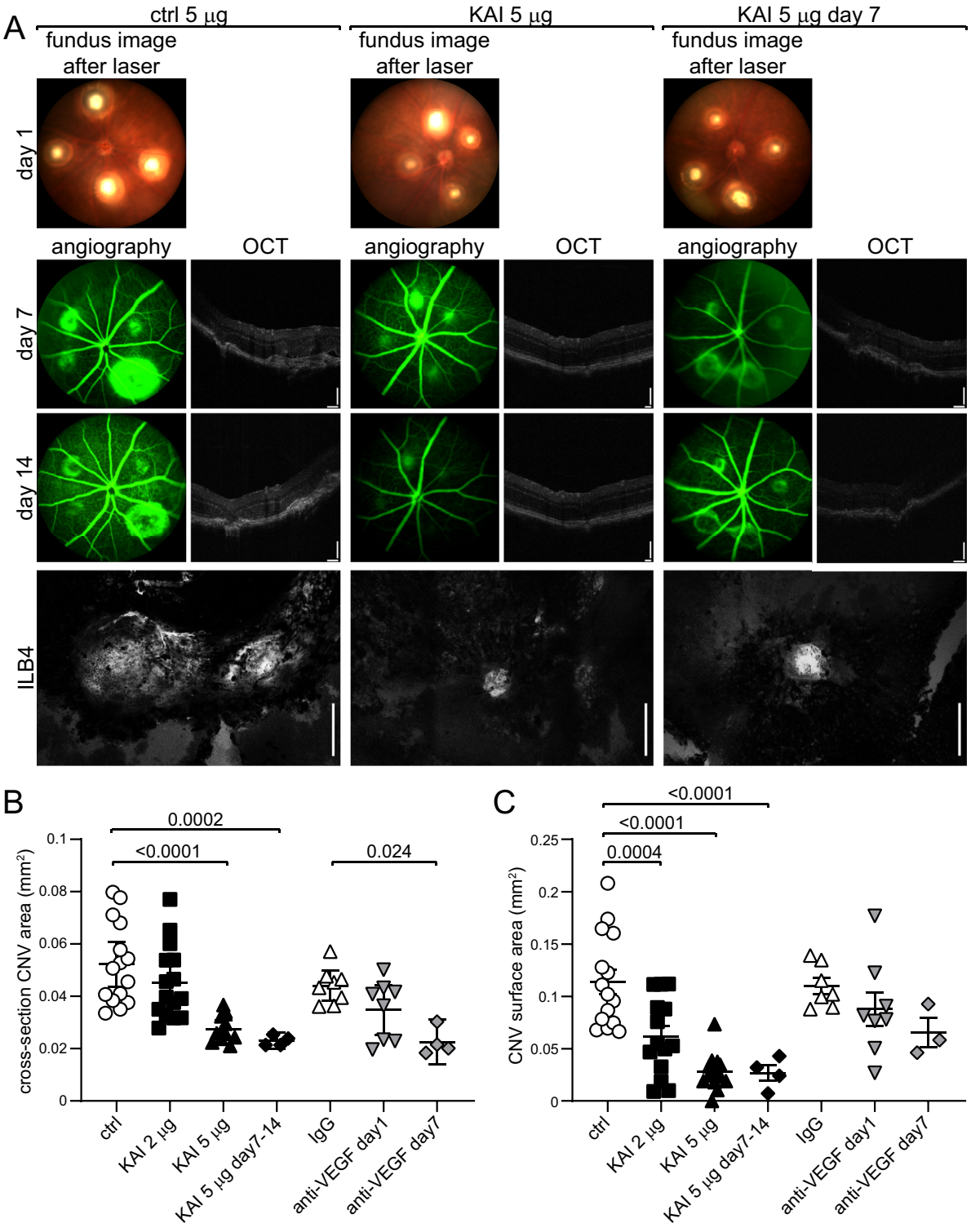

Figure 3. KAI eye drop shows efficacy to inhibit laser-induced CNV. (**A, B, C**) The effect of KAI as an eye drop was tested and compared with the effect of the intravitreal injection of anti-VEGF antibody in the CNV model. After laser photocoagulation, mice were treated with (1) control peptide (5 μg/eye) eye drop daily (days 1~14), (2) KAI (2 μg/eye) eye drop daily (days 1~14),(3) KAI (5 μg/eye) eye drop daily (days 1~14), (4) KAI (5 μg/eye) eye drop daily (days 7~14), (5) intravitreal injection of IgG 2 μg/eye at day 1, (6) intravitreal injection of anti-VEGF antibody 2 μg/eye at day 1, and (7) anti-VEGF antibody 2 μg/eye at day 7. (Groups 1~7 were plotted in graphs **B** and **C** starting from the left.) Representative images of the laser burn at day 1, OCT, and angiography at days 7 and 14, and staining of the flat-mount of choroid/sclera with ILB4 on day 14 were shown in **A** and Supplementary Figure S2. *Bars:* 100 μm for OCT, 200 μm for ILB4 staining. Four laser burns were induced in each mouse, and the average neovascularization area per mouse was shown in graphs **B** and **C**. The cross-section of the CNV area in OCT at day 14 was measured and plotted in graph **B**. One-way ANOVA ($N = 15, 15, 11, 4, 8, 8,$ and 4 in each group, respectively). Mice with mild cataract because of anesthesia were unable to be monitored by OCT and were omitted from the measurement. CNV surface area of the flat-mount was assessed by the area of ILB4-staining and plotted in graph **C**. One-way ANOVA ($N = 15, 14, 13, 4, 7, 8,$ and 3 in each group, respectively). Three choroidal tissues were damaged during the preparation of flat mount, and we were unable to assess the area of CNV. One-way ANOVA.

Investigative Ophthalmology & Visual Science

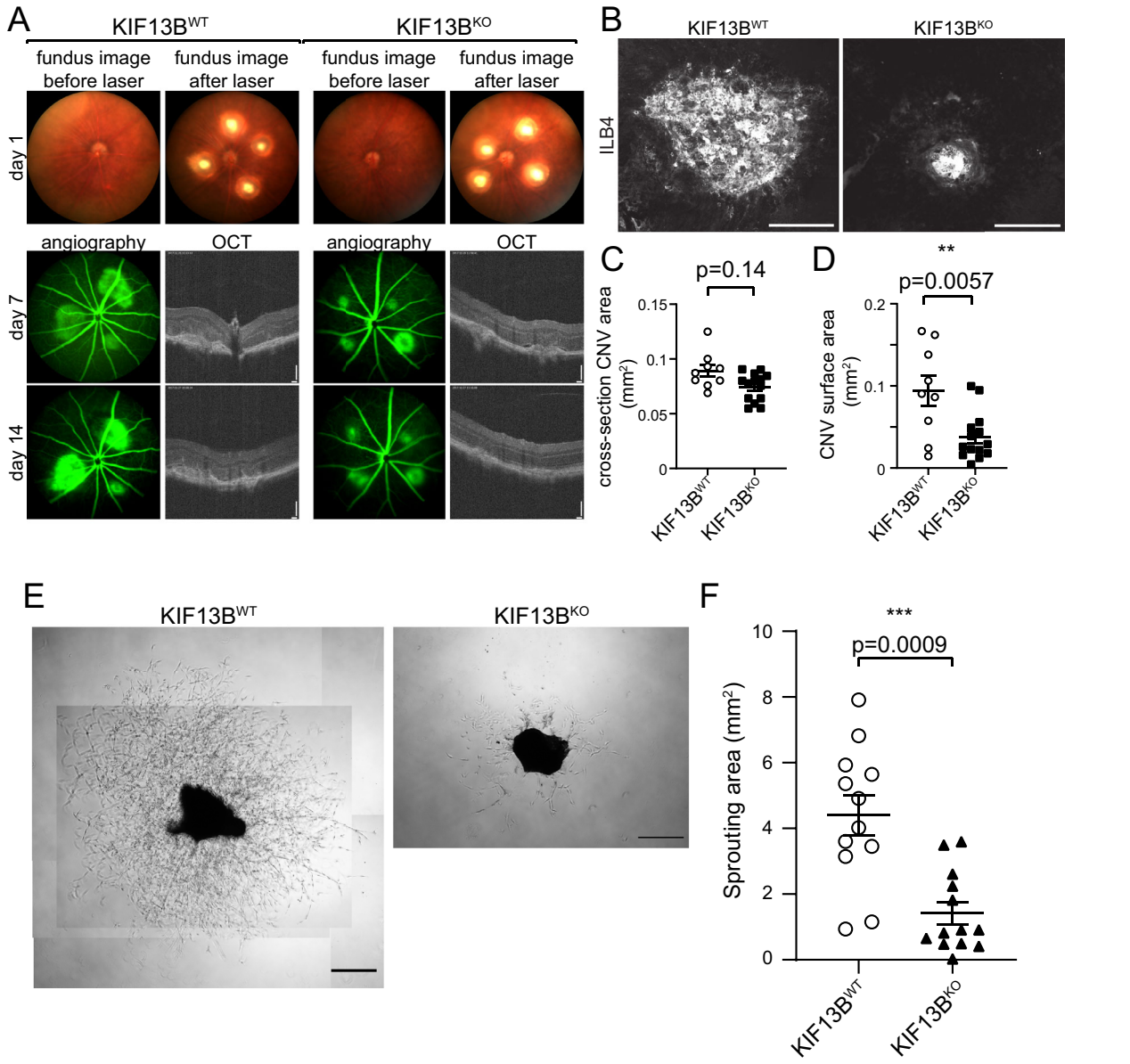

Figure 4. Genetically modified model of KIF13B knockout shows inhibition on laser-induced CNV and sprouting from choroidal vessels. (**A, B, C, D**) Impaired CNV in global KIF13B KO. *KIF13B*^{KO} and *WT* counterparts received laser burn. Representative images of fundus before and after laser burn at day 1, OCT and angiography at days 7 and 14 are shown in **A**. Representative image of the CNV lesion on flat-mount of choroid/sclera stained with DyLight594-ILB4 is shown in **B**. *Bars:* 100 µm for OCT, 200 µm for ILB4 staining. Four laser burns were induced in each mouse, and the average of neovascularization area per mouse is shown in graphs **C** and **D**. The cross-section of CNV area in OCT was measured and plotted in graph **C**. CNV surface area of the flat-mount was assessed by the area of ILB4-staining and plotted in graph **D**. Student's *t*-test ($N = 9$, 14 in *WT* and *KO*, respectively). (**E, F**) Inhibition of choroidal sprouting in *KIF13B*^{KO}. Choroidal tissues isolated from *KIF13B*^{WT} and *KIF13B*^{KO} (7 to 9 weeks old) were dissected and embedded into Matrigel. Seven days after embedding, the sprouting area from choroidal tissues was measured and shown in the graph as mean ± SE. The scatter plot represents the sprouting area from each choroidal tissue fragment. We dissected four to five pieces from each mouse and repeated the experiment three times ($N = 12$, 13 for *WT* and *KO*, respectively. N is the number of choroidal tissue fragments.) Representative images are shown. *Scale bars:* 500 µm.

A Genetic Model of KIF13B Knockout

To confirm the effect of inhibition of the function of KIF13B, we used a genetic model of KIF13B knockout (KO). KIF13B-floxed mice from the European Mouse Mutant Archive were crossed with flippase1 (flp1)-expressing mice, followed by crossing with CMV-Cre mice (The Jackson Laboratory) (Supplementary Fig. S3A). We confirmed the deletion of the KIF13B gene by genotyping (Supplementary Fig. S3B). KIF13B global KO was characterized as no gross anomalies and no apparent changes in the major organs. We have also examined the histology of the eyes of *KIF13B*^{WT} and *KIF13B*^{KO} by staining with VEGFR2, ILB4, GAD65, glutamine synthase, and rhodopsin (Supplementary Fig. S3C), but we did not see any difference between *KIF13B*^{KO} and *KIF13B*^{WT}.

Then, we tested *KIF13B*^{KO} and *KIF13B*^{WT} in laser-induced CNV (Fig. 4A). The fundus images in *KIF13B*^{KO} and *KIF13B*^{WT} (7 weeks old, female) were

indistinguishable before laser burn And they received similar sizes of laser burn (Fig. 4A). Angiography showed the inhibition of neovascularization *KIF13B*^{KO} compared to *KIF13B*^{WT} (Fig. 4A). The cross-section area of CNV at the lesion was shown by OCT (Figs. 4A, 4C). At 14 days after laser burn, the CNV surface area was measured by staining of the flat-mount of the choroid with DyLight 594-ILB4 (Figs. 4B, 4D). There was a statistically significant difference in CNV surface area between *KIF13B*^{KO} and *WT* counterpart, but not in the cross-section area.

In wet AMD, elevated expression of VEGF induces neovascularization from choroidal vessels.[7] To examine the effect of knockout of KIF13B in choroidal neovascularization, we used an ex vivo choroidal sprouting assay. First, to set up the ex vivo assay, choroidal tissue was isolated from the eyes of C57BL/6 and embedded in Matrigel.[30] Massive sprouting was grown even in the basal media supplemented with 2% FBS without additional growth factor supplements including FGF or VEGF (Supplementary Fig. S4A, left panel) due to the secretion of growth factors from the tissue. To confirm it is VEGF-dependent sprouting, we incubated the tissue with the anti-VEGF drug, Aflibercept. The sprouting was significantly inhibited by Aflibercept (Supplementary Fig. S4), suggesting the choroidal sprouting was induced by VEGF secreted from the tissue. Then, we tested sprouting from choroid isolated from the eyes of *KIF13B*^{WT} and *KIF13B*^{KO} in this condition (Figs. 4E, 4F). The area of sprouting on day 7 was measured and shown in the graph (Fig. 4F). The sprouting was significantly inhibited in *KIF13B*^{KO}, compared to *KIF13B*^{WT} control. The result suggests KIF13B is required for VEGF-induced choroidal neovascularization. Taken together, inhibition of KIF13B function by KAI can be a therapeutic strategy to inhibit neovascularization from choroidal vessels in wet AMD.

Discussion

We showed here that VEGFR2 trafficking can be a novel therapeutic target for wet AMD. The elevation of VEGF concentration in the eye fluid is the hallmark of wet AMD.[7] Because VEGF induces neovascularization of leaky vessels from choroidal vessels, which in turn causes inflammation and damage to the retina, anti-VEGF therapy is the current first-choice therapy.[7] To receive VEGF from tissue or fluid, VEGFR2 needs to be exposed to the cell surface. In our previous research, we found that a kinesin 3 family motor KIF13B is required to transport VEGFR2 to cell surface.[12] KIF13B directly interacts with VEGFR2; thus disruption of the interaction between KIF13B and VEGER2 by peptide KAI inhibits VEGF-induced EC migration, sprouting, and pathological angiogenesis in cancer models.[11] This article is the follow-up study to apply this strategy to angiogenesis-related eye disease, wet AMD.

Although KIF13B has multiple cargoes to regulate cell polarity and cell fate,[31,36–42] each cargo binds to a distinct domain of KIF13B (Fig. 1A). KAI was designed to specifically inhibit VEGFR2 binding, because KAI does not bind to the other cargo (Fig. 1B). From the mass spectrometry data, we found VEGFR2, NRP1, PDGFRα, PDGFRβ, and EGFR (Supplementary Fig. S1A). Although we found other tyrosine kinase receptors in mass spectrometry analysis, it does not mean their direct binding to KAI. Because the proteins were pulled down with KAI immobilized on the beads from the membrane fraction of the lung lysate, the proteins found there can be both direct binding and indirect binding. In addition, the possibility of nonspecific binding (false positive) cannot be avoided. Further direct analysis of SPR with synthesized peptides and recombinant proteins of receptor tyrosine kinases clarified the issue (Fig. 1C). SPR analysis confirmed the strong interaction of KAI with VEGFR2 with K_D 6.8 nM. The binding of KAI to other receptor tyrosine kinases was denied by SPR analysis, which further supports the specificity of KAI to VEGFR2.

Because KAI is a water-soluble small peptide (23 aa, 2.8 kD), topically applied KAI as an eye drop successfully delivered to the back of the eye (Fig. 2). Biotinylated KAI was detected by Alexa488-streptavidin. Endogenous biotin was an undetectable level in the eyes because no-peptide control did not show the fluorescence of Alexa488-streptavidin. Biotin-KAI was first visible at 30 min at the top of the retina, inner nuclear layer, outer nuclear layer, RPE, and choroidal vessels, suggesting successful delivery of the peptide. The peptide KAI was then cleared from the tissue, which was not surprising because peptide drugs usually have a short retention time.[43] Despite the short retention time, daily treatment of KAI was sufficient to inhibit neovascularization in the laser-induced CNV model (Fig. 3). Although the aqueous half-lives of intravitreal bevacizumab and ranibizumab in human eyes are 9.82 days and 7.19 days, respectively,[44,45] monthly injections of these anti-VEGF drugs effectively improve the vision of the patients. Thus the residual amount of drugs may retain the efficacy for a long period. In the case of KAI, the eye drop can be applied to human patients as frequently as possible to overcome the short retention time, thus it is not a critical weak point. Treatment of KAI eye drop showed reliable inhibition of CNV for almost all mice (Fig. 3). Comparing to the reliable result of eye drops, the variability of intravitreal injection of KAI (Fig. 1E, F) and anti-VEGF antibody was relatively higher. Although current therapy is effective to suppress angiogenesis and leakiness to improve vision in human patients,[2,4] current therapies require repeated intravitreal injection. There is a low risk of serious complications caused by the injections, such as retinal detachment, infection in the eyes, inflammation, and hemorrhage. Thus developing topically applicable therapy would be beneficial for patients with wet AMD. Nonetheless, more detailed pharmacokinetics of KAI in eye tissue and blood serum using bigger animals such as rabbits or monkeys, testing toxicity, and any adverse effects will be the future study.

Although anti-VEGF therapies are very effective to most of the wet AMD patients, some patients are still not responding.[8,9] Possible mechanisms causing decreased drug response in wet AMD could be changes in signal transduction to shift to the pathways under other growth factors, increased expression of VEGF from accumulated macrophages in damaged lesions in wet AMD, or increased expression of VEGFRs.[9] Thus switching the drugs between anti-VEGF antibodies and kinase inhibitors has been attempted to tackle nonresponsiveness.[8,10] Because our strategy is different from current therapies, it is possible to have a beneficial effect for nonresponders to current therapies. Combinational therapy is also another option if needed.

KAI is a pharmacological inhibitor for VEGFR2 trafficking in vitro.[11] On the other hand, knockdown of KIF13B inhibits VEGFR2 trafficking and VEGF-induced angiogenesis in vitro.[12] Thus, in this article, we used both pharmacological inhibitor and genetic deletion to confirm the effect of the inhibition of KIF13B -mediated VEGFR2 trafficking in laser-induced CNV. The CNV in *KIF13B*^{KO} was significantly

Investigative Ophthalmology & Visual Science

reduced compared to *WT* control (Figs. 4A–4D). KIF13B global KO was characterized as no gross anomalies and no apparent changes in the major organs.[40] We have also examined the histology of the eyes of $KIF13B^{WT}$ and $KIF13B^{KO}$ by staining with VEGFR2, ILB4, GAD65, glutamine synthase, and rhodopsin (Supplementary Fig. S3C), and the fundus image before applying laser burn (Fig. 4A), but we did not see any difference between $KIF13B^{KO}$ and $KIF13B^{WT}$. The structural change (for example, if there is any difference in the thickness of the Bruch's membrane) may affect the effectiveness of the laser burn; however, it is not likely the case, because we could not find any difference in $KIF13B^{WT}$ and $KIF13B^{KO}$. Thus the inhibition of CNV seen in $KIF13B^{KO}$ was not likely due to any developmental difference before the laser burn. After the laser burn, we observed that the disease progression was significantly less in $KIF13B^{KO}$. The disease progression in this model can be divided; early upregulation of VEGF from damaged tissue at day 3, leakage from the choroid to the retina at day 3,[46] inflammation and accumulation of neutrophils at days 1 to 3, and macrophages at days 3 to 5,[29] CNV and leakage at CNV lesion peaked at day 7.[29] We observed the mice at days 7 and 14 when the CNV was fully developed in control mice. WT control showed the increased thickness of the cross-section of CNV at the lesion and leaky CNV on day 7 and day 14, whereas these symptoms were reduced in $KIF13B^{KO}$. Because the phenotype is the neovascularization of choroidal vessels, we further confirmed it by ex vivo sprouting assay, where $KIF13B^{KO}$ significantly reduced VEGF-induced sprouting from choroidal tissue (Figs. 4E, 4F). On the basis of the previous mechanistic studies,[11,12] the simplest explanation is that the inhibition of KIF13B function by pharmacological inhibition or genetic deletion interferes with VEGFR2 trafficking, which is required for VEGF-induced angiogenesis in laser-induced CNV. Further investigation of the role of KIF13B on the early stage of the disease and the cell-types to affect will be the important future questions to define the further possibility of the efficacy of KAI on nonresponders for current therapies.

In summary, we demonstrated that the pharmacological inhibition of the interaction between KIF13B and VEGFR2 can be the therapeutic strategy to inhibit angiogenesis in wet AMD.

Acknowledgments

The authors are deeply grateful to Yulia Komarova and Victor H. Guaiquil for helpful suggestions to set up the laser-induced CNV model. We would like to thank Xiang Shen for technical advice for cryosection.

Supported by NIH grants R01 EY029339 (K.H.Y), NIH R56 HL128342 (K.H.Y.), RPB Stein Innovation Award (A.B.M.), and UIC Chancellor's Innovation Fund (K.H.Y.).

Disclosure: **S.B. Waters,** None; **C. Zhou,** None; **T. Nguyen,** None; **R. Zelkha,** None; **H. Lee,** None; **A. Kazlauskas,** None; **M.I. Rosenblatt,** None; **A.B. Malik,** None; **K.H. Yamada,** None

References

1. Folkman J. Angiogenesis: an organizing principle for drug discovery? *Nat Rev Drug Discov*. 2007;6:273–286.
2. Potente M, Gerhardt H, Carmeliet P. Basic and therapeutic aspects of angiogenesis. *Cell*. 2011;146:873–887.
3. Ferrara N, Hillan KJ, Gerber HP, Novotny W. Discovery and development of bevacizumab, an anti-VEGF antibody for treating cancer. *Nat Rev Drug Discov*. 2004;3:391–400.
4. Crawford Y, Ferrara N. VEGF inhibition: insights from preclinical and clinical studies. *Cell Tissue Res*. 2009;335:261–269.
5. Crawford Y, Ferrara N. Tumor and stromal pathways mediating refractoriness/resistance to anti-angiogenic therapies. *Trends Pharmacol Sci*. 2009;30:624–630.
6. Chen HX, Cleck JN. Adverse effects of anticancer agents that target the VEGF pathway. *Nat Rev Clin Oncol*. 2009;6:465–477.
7. Ferrara N. Vascular endothelial growth factor and age-related macular degeneration: from basic science to therapy. *Nat Med*. 2010;16:1107–1111.
8. Ehlken C, Jungmann S, Böhringer D, Agostini HT, Junker B, Pielen A. Switch of anti-VEGF agents is an option for nonresponders in the treatment of AMD. *Eye (Lond)*. 2014;28:538–545.
9. Binder S. Loss of reactivity in intravitreal anti-VEGF therapy: tachyphylaxis or tolerance? *Br J Ophthalmol*. 2012;96:1–2.
10. Nagai N, Suzuki M, Uchida A, et al. Non-responsiveness to intravitreal aflibercept treatment in neovascular age-related macular degeneration: implications of serous pigment epithelial detachment. *Sci Rep*. 2016;6:29619.
11. Yamada KH, Kang H, Malik AB. Antiangiogenic therapeutic potential of peptides derived from the molecular motor KIF13B that transports VEGFR2 to plasmalemma in endothelial cells. *Am J Pathol*. 2017;187:214–224.
12. Yamada KH, Nakajima Y, Geyer M, et al. KIF13B regulates angiogenesis through Golgi to plasma membrane trafficking of VEGFR2. *J Cell Sci*. 2014;127:4518–4530.
13. Gampel A, Moss L, Jones MC, Brunton V, Norman JC, Mellor H. VEGF regulates the mobilization of VEGFR2/KDR from an intracellular endothelial storage compartment. *Blood*. 2006;108:2624–2631.
14. Hayashi M, Majumdar A, Li X, et al. VE-PTP regulates VEGFR2 activity in stalk cells to establish endothelial cell polarity and lumen formation. *Nat Commun*. 2013;4:1672.
15. Lanahan AA, Hermans K, Claes F, et al. VEGF receptor 2 endocytic trafficking regulates arterial morphogenesis. *Dev Cell*. 2010;18:713–724.
16. Manickam V, Tiwari A, Jung J-J, et al. Regulation of vascular endothelial growth factor receptor 2 trafficking and angiogenesis by Golgi localized t-SNARE syntaxin 6. *Blood*. 2011;117:1425–1435.
17. Simons M, Gordon E, Claesson-Welsh L. Mechanisms and regulation of endothelial VEGF receptor signalling. *Nat Rev Mol Cell Biol*. 2016;17:611–625.
18. Nakayama M, Nakayama A, van Lessen M, et al. Spatial regulation of VEGF receptor endocytosis in angiogenesis. *Nat Cell Biol*. 2013;15:249–260.
19. Lampugnani MG, Orsenigo F, Gagliani MC, Tacchetti C, Dejana E. Vascular endothelial cadherin controls VEGFR-2 internalization and signaling from intracellular compartments. *J Cell Biol*. 2006;174:593–604.
20. Ewan LC, Jopling HM, Jia H, et al. Intrinsic tyrosine kinase activity is required for vascular endothelial growth factor receptor 2 ubiquitination, sorting and degradation in endothelial cells. *Traffic*. 2006;7:1270–1282.
21. Bruns AF, Herbert SP, Odell AF, et al. Ligand-stimulated VEGFR2 signaling is regulated by co-ordinated trafficking and proteolysis. *Traffic*. 2010;11:161–174.
22. Jopling HM, Odell AF, Hooper NM, Zachary IC, Walker JH, Ponnambalam S. Rab GTPase regulation of VEGFR2 trafficking and signaling in endothelial cells. *Arterioscler Thromb Vasc Biol*. 2009;29:1119–1124.

23. Simons M. An inside view: VEGF receptor trafficking and signaling. *Physiology*. 2012;27:213–222.
24. Yamaoka-Tojo M, Ushio-Fukai M, Hilenski L, et al. IQGAP1, a novel vascular endothelial growth factor receptor binding protein, is involved in reactive oxygen species–dependent endothelial migration and proliferation. *Circ Res*. 2004;95:276–283.
25. Gerhardt H, Golding M, Fruttiger M, et al. VEGF guides angiogenic sprouting utilizing endothelial tip cell filopodia. *J Cell Biol*. 2003;161:1163–1177.
26. Jakobsson L, Franco CA, Bentley K, et al. Endothelial cells dynamically compete for the tip cell position during angiogenic sprouting. *Nat Cell Biol*. 2010;12:943–953.
27. Hirokawa N, Noda Y, Tanaka Y, Niwa S. Kinesin superfamily motor proteins and intracellular transport. *Nat Rev Mol Cell Biol*. 2009;10:682–696.
28. Gong Y, Li J, Sun Y, et al. Optimization of an image-guided laser-induced choroidal neovascularization model in mice. *PLoS One*. 2015;10:e0132643.
29. Lambert V, Lecomte J, Hansen S, et al. Laser-induced choroidal neovascularization model to study age-related macular degeneration in mice. *Nat Protoc*. 2013;8:2197–2211.
30. Shao Z, Friedlander M, Hurst CG, et al. Choroid sprouting assay: an ex vivo model of microvascular angiogenesis. *PLoS One*. 2013;8:e69552.
31. Horiguchi K, Hanada T, Fukui Y, Chishti AH. Transport of PIP3 by GAKIN, a kinesin-3 family protein, regulates neuronal cell polarity. *J Cell Biol*. 2006;174:425–436.
32. Saint-Geniez M, Maldonado AE, D'Amore PA. VEGF expression and receptor activation in the choroid during development and in the adult. *Invest Ophthalmol Vis Sci*. 2006;47:3135–3142.
33. Yuo-Sheng C, Chwen-Huey W, Re-Jiin C,, Shiuan D. Determination of biotin concentration by a competitive enzyme-linked immunosorbent assay (ELISA) method. *J Biochem Biophys Methods*. 1994;29:321–329.
34. CATT Research Group,Martin DF, Maguire MG, et al. Ranibizumab and bevacizumab for neovascular age-related macular degeneration. *N Engl J Med*. 2011;364:1897–1908.
35. Rosenfeld PJ, Brown DM, Heier JS, et al. Ranibizumab for neovascular age-related macular degeneration. *N Engl J Med*. 2006;355:1419–1431.
36. Yamada KH, Hanada T, Chishti AH. The effector domain of human Dlg tumor suppressor acts as a switch that relieves autoinhibition of kinesin-3 motor GAKIN/KIF13B. *Biochemistry*. 2007;46:10039–10045.
37. Schou KB, Mogensen JB, Morthorst SK, et al. KIF13B establishes a CAV1-enriched microdomain at the ciliary transition zone to promote Sonic hedgehog signalling. *Nature Communications*. 2017;8:14177.
38. Noseda R, Guerrero-Valero M, Alberizzi V, et al. Kif13b regulates PNS and CNS myelination through the Dlg1 scaffold. *PLoS Biol*. 2016;14:e1002440.
39. Liao EH, Gray L, Tsurudome K, et al. Kinesin Khc-73/KIF13B modulates retrograde BMP signaling by influencing endosomal dynamics at the Drosophila neuromuscular junction. *PLoS Genet*. 2018;14:e1007184.
40. Kanai Y, Wang D, Hirokawa N. KIF13B enhances the endocytosis of LRP1 by recruiting LRP1 to caveolae. *J Cell Biol*. 2014;204:395–408.
41. Jenkins B, Decker H, Bentley M, Luisi J, Banker G. A novel split kinesin assay identifies motor proteins that interact with distinct vesicle populations. *J Cell Biol*. 2012;198:749–761.
42. Hanada T, Lin L, Tibaldi EV, Reinherz EL, Chishti AH. GAKIN, a novel kinesin-like protein associates with the human homologue of the Drosophila discs large tumor suppressor in T lymphocytes. *J Biol Chem*. 2000;275:28774–28784.
43. Mandal A, Pal D, Agrahari V, Trinh HM, Joseph M, Mitra AK. Ocular delivery of proteins and peptides: challenges and novel formulation approaches. *Adv Drug Deliv Rev*. 2018;126:67–95.
44. Krohne TU, Liu Z, Holz FG, Meyer CH. Intraocular pharmacokinetics of ranibizumab following a single intravitreal injection in humans. *Am J Ophthalmol*. 2012;154:682–686.
45. Krohne TU, Eter N, Holz FG, Meyer CH. Intraocular pharmacokinetics of bevacizumab after a single intravitreal injection in humans. *Am J Ophthalmol*. 2008;146:508–512.
46. Fantin A, Lampropoulou A, Senatore V, et al. VEGF165-induced vascular permeability requires NRP1 for ABL-mediated SRC family kinase activation. *J Exp Med*. 2017;214:1049–1064.

Investigative Ophthalmology & Visual Science